NEUTRINO-LEPTON INTERACTIONS FOR QUANTUM COMPUTING

M. Cullen
Loughborough University
United Kingdom
(Dated: March 28, 2022)

One of the largest problems quantum computing development has faced, would be the loss of quantum information as systems scale. Here we investigate the use of neutrino flavor states as qubit states where we propose neutrino-lepton interactions for the realisation of a universal set of qubit manipulations and concluded that such a quantum computer is not probable and the resources required is unfeasible.

I. INTRODUCTION

The idea of quantum computing has been around since the formation of quantum mechanics itself making use of quantum entanglement and teleportation techniques. This in turn led to experimental multi qubit systems to be developed in the 90's, using a variety of methods such as NMR and quantum annealing. Research then began to adopt more universal quantum computing methods using superconducting qubits, spin based silicon qubits and quantum computing using only linear optical components [1–4]. The largest problem all these systems faced and still face, concern decoherence while scaling where quantum information is lost as we try to increase the number of qubits in a system.

In this paper we decide to take a step back from the conventional methods of quantum computing and take a look at using neutrinos as quantum bits. The discovery of neutrino mass and hence flavor superposition, allow neutrinos to exhibit the quantum properties necessary for a multi qubit system. Neutrino flavors can correspond to various states due to different mass states and flavor and mass superposition gives an intrinsic probabilistic Hadamard gate that depends on distance propagated. The neutrinos abundance and elusive nature show potential for easier initialisation and scaling, where conventional methods lack.

II. FRAMEWORK

To develop a theoretical framework of neutrinos as qubits, we need to follow D. DiVincenzo's outlines for the requirements to create a quantum computer [5];

- 1. A scalable physical system with well characterized qubits,
- 2. The ability to initialize the state of the qubits to a simple fiducial state, such as $|000...\rangle$,
- 3. Long relevant decoherence times, much longer than the gate operation time,
- 4. A "universal" set of quantum gates,
- 5. A qubit-specific measurement capability.

Points 1 and 2 require neutrino beams that can reliably initialise a large number of same state neutrinos. Neutrino beams are addressed in more detail in the "Initialisation" section.

In point 3 a neutrinos main source of decoherence will be during atmospheric travel and these values need to be compared to gate operation times. As our gates consist of neutrino-lepton interactions; neutrino's decohering faster than lepton interactions can complete is not a large concern.

Point 4 is the main focus of this project, where we formalise our quantum gates as neutrino-lepton interactions; which invoke quantum state changes. As we are using neutrino-lepton interactions we can have qubit-specific measurements of the other lepton products that are produced.

III. NEUTRINOS AND QUANTUM COMPUTING

A. Quantum Mechanical Representation

Neutrino oscillations were theorised and predicted by Pontecorvo in 1957 and contributed as a solution to the solar neutrino problems of the 1960's where work from Super Kamiokande, Sudbury, CERN and others have helped verify the existence of neutrino flavor states and the oscillatory properties connecting them [6–8].

The quantum mechanical representation of neutrino mass states, describing a superposition of neutrino flavor states can be denoted by;

$$\begin{aligned} |\nu_\alpha\rangle &= cos\theta\,|\nu_e\rangle + sin\theta\,|\nu_\mu\rangle \\ |\nu_\beta\rangle &= -sin\theta\,|\nu_e\rangle + cos\theta\,|\nu_\mu\rangle \end{aligned} \tag{1}$$

where in quantum computation, a two flavor neutrinos qubit basis can be written as;

$$\begin{aligned} |0\rangle = |\nu_e\rangle &= \begin{bmatrix} 1 \\ 0 \end{bmatrix} \\ |1\rangle = |\nu_\mu\rangle &= \begin{bmatrix} 0 \\ 1 \end{bmatrix} \end{aligned} \tag{2}$$

where rotation between the basis and flavor basis is performed via a unitary matrix $U^{2x2}_{PMNS}(2\theta, \phi, \lambda)$, with $\phi = \lambda = 0$;

$$U^{2x2}_{PMNS}(2\theta, 0, 0) = \begin{bmatrix} cos(\theta) & -sin(\theta) \\ sin(\theta) & cos(\theta) \end{bmatrix} \tag{3}$$

$$\begin{aligned} |\nu_\alpha\rangle &= U^{2x2}_{PMNS} |\nu_e\rangle \\ |\nu_\beta\rangle &= U^{2x2}_{PMNS} |\nu_\mu\rangle \end{aligned} \tag{4}$$

For a three flavor basis, we have a variation in our PMNS matrix however it acts the same on our three flavor basis;

$$\begin{aligned} |\nu_\alpha\rangle &= U^{3x3}_{PMNS} |\nu_e\rangle \\ |\nu_\beta\rangle &= U^{3x3}_{PMNS} |\nu_\mu\rangle \\ |\nu_\gamma\rangle &= U^{3x3}_{PMNS} |\nu_\tau\rangle \end{aligned} \tag{5}$$

The U^{3x3}_{PMNS} matrix is less trivial than U^{2x2}_{PMNS}, but has been derived to Eq. 6 and has been modelled and verified by IBM-Q in "Neutrino Oscillations in a Quantum Processor" [9];

$$U^{3x3}_{PMNS} = \begin{bmatrix} 1 & 0 & 0 \\ 0 & cos\theta_{\beta\gamma} & sin\theta_{\beta\gamma} \\ 0 & -sin\theta_{\beta\gamma} & cos\theta_{\beta\gamma} \end{bmatrix} * \begin{bmatrix} cos\theta_{\alpha\gamma} & 0 & sin\theta_{\alpha\gamma} e^{i\delta_{cp}} \\ 0 & 1 & 0 \\ -sin\theta_{\alpha\gamma} & 0 & cos\theta_{\alpha\gamma} \end{bmatrix} * \begin{bmatrix} cos\theta_{\alpha\beta} & sin\theta_{\alpha\beta} & 0 \\ -sin\theta_{\alpha\beta} & cos\theta_{\alpha\beta} & 0 \\ 0 & 0 & 1 \end{bmatrix} * \begin{bmatrix} 1 & 0 & 0 \\ 0 & e^{i\Psi} & 0 \\ 0 & 0 & e^{i\Gamma} \end{bmatrix} \tag{6}$$

U^{3x3}_{PMNS} performs rotation via the first three matrices with CP parity included in matrix 3. Matrix 4 has no effect on neutrino oscillations as it is believed that Majorana phases have no effect on oscillations.

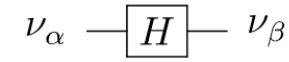

FIG. 1. show the gate interaction for an input and output neutrino where the flavor oscillation acts as a one qubit Hadamard gate.

B. Neutrino Oscillation

The probability of neutrino oscillation between three flavors is given by;

$$P_{\nu_\alpha \to \nu_\beta} = sin^2(2\theta) sin^2(\frac{\Delta m^2_{\alpha\beta} L}{4E}) \tag{7}$$

where $\Delta m_{\alpha\beta}$ is the mass difference between the two neutrino mass states. The oscillation probability as a function of oscillation distance, for all flavor states, is shown in Fig 5.

The oscillation probability depends on the neutrinos distance travelled over neutrino energy, where we can get predictable oscillation probabilities by fixing our distance to be the distance between the emitter and detector and emitting neutrinos at a constant energy. This ideally reduces the variation in oscillation probability and the forcing to undesirable flavors while also being used to calculate the probability of superposition; with propagation through space acting as a Hadamard gate. This is our natural one-qubit gate, shown in Fig 1.

C. Initialisation

Point 2 of DiVincenzo's outlines require reliable initialisation of the $|000...\rangle$ states. By using methods that generate specific flavor neutrino beams we can initialise our quantum states. For instance, Fermilab creates neutrino beams for their various experiments such as in their BNB (booster neutrino beamline). They start with a tank of negatively charged and accelerated hydrogen which strips into protons. Smashing the protons into a graphite target produces pions and kaons, which are then funnelled by electromagnetic fields and decay into neutrinos, electrons, and muons [10, 11].

Short lived kaons largely decay into two pions which then decay according to;

$$\begin{aligned} \pi^+ &\to \mu^+ + \nu_\mu \\ \pi^- &\to \mu^- + \overline{\nu_\mu} \end{aligned} \tag{8}$$

The pion decay branch that leads to muon neutrinos has a branching ratio of 0.999877 where the electron neutrino branching ratio is 0.000123 [12];

$$\begin{aligned} \pi^+ &\to e^+ + \nu_e \\ \pi^- &\to e^- + \overline{\nu_e} \end{aligned} \tag{9}$$

Isolating the neutrinos is done by passing the products through walls of steel and concrete as this will absorb the electrons and muons and allow the neutrinos to freely pass.

IV. INTERACTIONS

A. CNOT Gate

A "universal" set of quantum gates is the main focus of this paper, where we have decided to investigate the possible fundamental neutrino-lepton interactions that may represent a CNOT gate in particular. Fig 6 show Feynman diagrams of neutrinos interacting with electrons; providing a start for developing our potential quantum gates.

We can describe a two qubit gate as two input neutrinos, undergoing lepton interactions, and two outgoing neutrino flavors dependant on the results of the interaction. We can calculate the individual and combined cross sections of each interaction; leading to complete gate probabilities.

B. Muons

Using neutrinos and anti-neutrinos together as inputs result in an incomplete CNOT truth table as they cannot transition between neutrino and anti-neutrino states. This rules out using the mixture of the two until neutrinos can be confirmed to act as Majorana particles. In fact, solely using electrons as targets would result in an incomplete CNOT truth table for all initial states, as interactions for ν_e to ν_μ and $\overline{\nu}_\mu$ to $\overline{\nu}_e$ are not possible.

Fig 2 introduces muons, μ^-, as targets, allowing for the above transitions. Muon targets are short lived, ≈ 2.197 μs, and their most common decay path, $\mu^- \rightarrow e^- \overline{\nu}_e \nu_\mu$, contributes to added complexity as it does not allow us to isolate desired neutrino flavors and leptons.

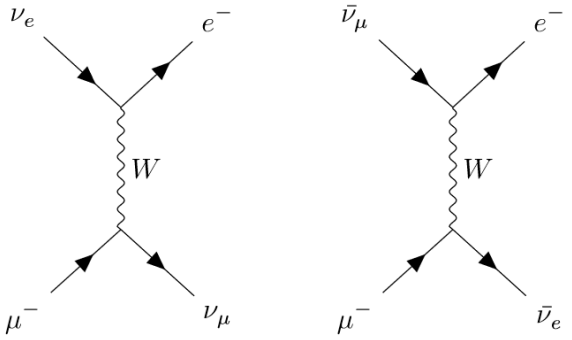

FIG. 2. Feynman diagram interactions of electron neutrino and muon anti-neutrino with target muons.
(a) $\nu_e + \mu^- \rightarrow e^- + \nu_\mu$, (b) $\overline{\nu}_\mu + \mu^- \rightarrow e^- + \overline{\nu}_e$.

These experimental difficulties will require constant feedback and filtering of undesired elements in the gate, allowing for interaction probabilities to be more consistent. To account for muon decay rate effects, increasing the number of targets allows for decay probability and decay elements to be consistent and can be accounted for. Furthermore, a constant decay rate and loss of muon targets allows for pumping of additional target muons at the same rate as they decay (Γ_μ), where over a large number of particles the decay rates should have negligible effect on cross section probabilities.

$$\Gamma_\mu = \frac{G_F^2 m_\mu^5}{192\pi^3} \tag{10}$$

Muons decaying into specific neutrino flavors complicates the gate inputs and outputs as the neutrino decay products will also interact and can only be avoided by following strict input and output vectors angles to be able to differentiate between wanted and unwanted neutrinos.

C. Cross Sections

To describe the cross-sections we refer to MIT and Fermilabs "From eV to EeV: Neutrino cross sections across energy scales", where they give a detailed kinematic approach of producing cross-section equations that agree well with experimental data [13].

Considering both the NC and CC interactions we can generalise our cross sections. To do this both NC and CC lepton charged current parts are needed:

$$\begin{aligned} NC &: j_Z^\mu = 2 \sum_{\alpha=e,\mu,\tau} g_L^\nu \overline{\nu}_{\alpha L} \gamma^\mu \nu_{\alpha L} + g_L^f \bar{l}_{\alpha L} \gamma^\mu l_{\alpha L} + g_R^f \bar{l}_{\alpha R} \gamma^\mu l_{\alpha R} \\ CC &: j_W^\mu = 2 \sum_{\alpha=e,\mu,\tau} \overline{\nu}_{\alpha L} \gamma^\mu l_{\alpha L} \end{aligned} \tag{11}$$

where $\nu_{\alpha L(R)}$ and $l_{\alpha L(R)}$ represent the left and right handed lepton field components, γ^μ represents the gamma matrices $\{\gamma^0, \gamma^1, \gamma^2, \gamma^3\}$ and $g_{L/R}^{\mu/f}$ represent the fermion coupling constants. This leads to Lagrangian formalism for both NC and CC, via boson couplings:

$$\begin{aligned} \mathcal{L}_{NC} &= -\frac{g}{2cos(\theta_W)} j_Z^\mu Z_\mu \\ \mathcal{L}_{CC} &= -\frac{g}{2\sqrt{2}}(j_W^\mu W_\mu + j_W^{\mu\dagger} W_\mu^\dagger) \end{aligned} \tag{12}$$

where W_μ and Z_μ represent the heavy boson fields, θ_W represents the coupling constant (Weinberg angle) and g represents the weak mixing angle.

With the Lagrangian and Feynman diagram matrix formalism it is possible to represent all neutrino interactions [14].

We arrive at the differential cross section with respect to outgoing lepton energy:

$$\frac{d\sigma(\nu_l \to \nu_e l)}{dy} = \frac{2m_e G_F^2 E_\nu}{\pi}(1 - \frac{m_l^2 - m_e^2}{2m_e E_\nu}) \tag{13}$$

Eq 13 is the basis of representing the integrated cross sections for neutrino-electron scattering in Fig 3.

Reaction	Type	$\sigma(E_\nu \gg E_{\text{thresh}})/\sigma_0$
$\nu_e e^- \to \nu_e e^-$	CC and NC	$\frac{1}{4} + \sin^2\theta_W + \frac{4}{3}\sin^4\theta_W$
$\bar{\nu}_e e^- \to \bar{\nu}_e e^-$	CC and NC	$\frac{1}{12} + \frac{1}{3}\sin^2\theta_W + \frac{4}{3}\sin^4\theta_W$
$\bar{\nu}_e e^- \to \bar{\nu}_\mu \mu^-$	CC	$\frac{1}{3}$
$\nu_\mu e^- \to \nu_e \mu^-$	CC	1
$\nu_\mu e^- \to \nu_\mu e^-$	NC	$\frac{1}{4} - \sin^2\theta_W + \frac{4}{3}\sin^4\theta_W$
$\bar{\nu}_\mu e^- \to \bar{\nu}_\mu e^-$	NC	$\frac{1}{12} - \frac{1}{3}\sin^2\theta_W + \frac{4}{3}\sin^4\theta_W$

FIG. 3. Fermilabs table shows the integrated cross section for neutrino-lepton scattering interactions as a function of the asymptotic cross-section and fermion field coupling constants (does not account for corrections due to leptonic masses and radiative correlations) [13].

This table shows the integrated cross sections of neutrino-lepton interactions for the charged current and neutral current interactions (or both) that are being considered. All cross-sections are compared to the inverse beta decay asymptotic cross-section (σ_0) from radioactive and fission reactors being experimentally well understood and measured;

$$\sigma_0 = \frac{G_F^2 s_{\nu_l,e}}{\pi} = 1.72 \times 10^{-45} \frac{m^2}{GeV} \tag{14}$$

$$s_{\nu_l,e} = (\rho_\nu + \rho_e)^2 \tag{15}$$

with experimental fission values being to the same order [15];

$$\begin{aligned} \sigma_{Bugea-4} &= 5.75(\pm 0.08) \times 10^{-45} m^2/fission \\ \sigma_{DayaBay} &= 5.92(\pm 0.14) \times 10^{-45} m^2/fission \end{aligned} \tag{16}$$

However, our neutrinos ideally have a lot more energy; ≈ 100 GeV. Therefore our asymptotic cross section should be larger than the experimentally verified values;

$$\begin{aligned} \sigma_{0,e} &\approx \frac{2m_e G_F^2 E_\nu}{\pi} = 4.426 \times 10^{-12} \frac{m^2}{GeV} \\ \sigma_{0,\mu} &\approx \frac{2m_\mu G_F^2 E_\nu}{\pi} = 9.094 \times 10^{-10} \frac{m^2}{GeV} \end{aligned} \tag{17}$$

G_F is the Fermi coupling constant and $s \approx 2m_e E_\nu$ is the center of mass energy of this asymptotic interaction [16]. By combining the asymptotic cross-section (σ_0) with the fermion field coupling constant equations (Fig 3) we can approximate the gate probabilities as a function of the incoming neutrino energy E_ν.

Following these same principles we can determine the neutrino-muon cross sections based on the neutrino-electron cross sections above. The important difference between the electron and the muon would be the much greater muon mass; $m_\mu = 0.105$ GeVc^{-2} and $m_e = 0.511 \times 10^{-3}$ GeVc^{-2}. The muon and electron, however, share the same leptonic coupling constants as shown in Fig 4. Instead the mass difference effects the kinematic elements in our derivation;

$$s_{\nu_l,\mu} = (\rho_\nu + \rho_\mu)^2 \tag{18}$$

$$\sigma_0 = \frac{G_F^2 s_{\nu_l,\mu}}{\pi} \tag{19}$$

Fermion	g_L^f	g_R^f	g_V^f	g_A^f
ν_e, ν_μ, ν_τ	$+\frac{1}{2}$	0	$+\frac{1}{2}$	$+\frac{1}{2}$
e, μ, τ	$-\frac{1}{2} + \sin^2\theta_W$	$+\sin^2\theta_W$	$-\frac{1}{2} + 2\sin^2\theta_W$	$-\frac{1}{2}$
u, c, t	$+\frac{1}{2} - \frac{2}{3}\sin^2\theta_W$	$-\frac{2}{3}\sin^2\theta_W$	$+\frac{1}{2} - \frac{4}{3}\sin^2\theta_W$	$+\frac{1}{2}$
d, s, b	$-\frac{1}{2} + \frac{1}{3}\sin^2\theta_W$	$+\frac{1}{3}\sin^2\theta_W$	$-\frac{1}{2} + \frac{2}{3}\sin^2\theta_W$	$-\frac{1}{2}$

FIG. 4. Fermilabs table shows the values for the g_V (vector), g_A (axial), g_L (left), and g_R (right) coupling constants for the known fermion fields [13].

D. Mass Suppression

Now that we are considering electrons and muons as targets, mass suppression (ξ) has to be taken into account as certain interaction probabilities are suppressed

more dependant on lepton mass. Furthermore, it is expected that due to the muons much higher mass the corresponding neutrino cross sections will dominate the electron cross sections without considering mass suppression.

$$\xi = 1 - \frac{m_{out}^2}{m_{in}^2 + 2m_{in}E_\nu} \tag{20}$$

ξ is the fraction in which the cross section is suppressed by, allowing for cross sections that account for varying lepton mass [16].

This also sets a threshold on the neutrino energy reactions where there is a target electron and an output muon, such as the IBD reaction shown in Fig 6(d), resulting in $E_\nu > 11$ GeV. On average there is a $< 1\%$ difference in mass suppression between our neutrino-electron or neutrino-muon interactions at our 100 GeV neutrino energies.

E. Results

The combination of electron and muon targets allows for a complete CNOT truth table with Table I showing the probabilities of each CNOT output occurring;
A variety of different outputs for each input are probable and a unitary CNOT gate wants the desired output as the most probable interaction. Instead only one of our CNOT outputs happen to be the most probable where the most probable outputs and their respective probabilities can be clearly compared to the desired outputs and probabilities in Table I (universal CNOT gate probabilities).

Input (a & b)	Desired Output	Probable Output	Desired Probability	Probable Probability
ee	ee	eμ / μe	6.07×10^{-16}	2.24×10^{-15}
eμ	eμ	eμ	1.05×10^{-16}	1.05×10^{-16}
μe	$\mu\mu$	μe	3.88×10^{-16}	1.05×10^{-16}
$\mu\mu$	μe	$\mu\mu$	1.89×10^{-18}	1.82×10^{-17}

TABLE I. CNOT truth table showing the desired outputs and probable outputs, accompanied with their respective probabilities, for $E_\nu = 100$ GeV (considering $|0\rangle = |e\rangle = |\nu_e\rangle$ and $|1\rangle = |\mu\rangle = |\nu_\mu\rangle$).

Regardless of the input states for ν_e and ν_μ, the most probable output state is not the desired output state for a CNOT gate. Furthermore, when deciding to change our states $|0\rangle$ and $|1\rangle$ to anti-neutrino states, we encounter a similar problem where the most probable output state mainly tends towards $|\overline{e}\overline{e}\rangle$. This is largely due to the introduction of neutrino-muon interactions being the most dominating interaction by a few orders of magnitude; even while considering mass suppression.

Therefore our derived neutrino-lepton gate fails to fulfill the requirements as a universal two qubit CNOT due to our gate most likely outputting an incorrect state when it does undergo interaction.

V. IMPROVING PROBABILITIES

As we are considering probabilistic gates we can liken them to linear optical quantum computing theories that use photons as qubits [4]. If we were to consider a two qubit gate possible we would have to improve our probabilities drastically where our predicted gate cross-sections are of the order 10^{-16} on average for 100GeV neutrinos; posing a large problem for using neutrinos as qubits as operations are not likely to occur.

To grasp how large a task improving these rates is, let us entertain ways we can approach P $\approx$ 1. To improve these cross-sections, we can increase the number of neutrinos, increase the number of gates/targets or increase the incoming neutrino energies.

To increase the neutrino energies by 10^{15} we reach intergalactic neutrino energy scales. Already 100 GeV was a very high initial value to consider for these interactions but increasing this by 10^{15} is unfeasible. If we decide to increase the number of neutrinos by using the number of neutrinos passing through the Earth every second (10^{14}) we would be off by a factor of 10^1. For similar reasons, increasing the number of gates/targets is difficult as neutrinos are much more abundant than the materials it would take to build these gates. A combination of all three is still an incredibly difficult task resulting in unfeasible numbers.

A. Using Best Values

However, let us put it into perspective by improving our probabilities with the use of stars and Dyson spheres to capture a larger neutrino flux.

Taking our Sun as a reference, there are $\phi = 7 \times 10^7 m^{-2} s^{-1}$ neutrinos incident on the Earth. Using a simple flux calculation for N (number of neutrinos the Sun emits per second);

$$\begin{aligned} \phi &= \frac{N}{4\pi r^2} \\ N &= \phi 4\pi r^2 \\ N &= 7 \times 10^7 \times 4\pi \times (1.5 \times 10^{11})^2 \\ N &\approx 2 \times 10^{31} s^{-1} \end{aligned} \tag{21}$$

where ϕ is the neutrino flux at the Earth ($m^{-2}s^{-1}$), and r is the distance from the Sun to the Earth.

These neutrinos will be radiating out from the star and will not all be focused towards our gates. If we wish to find a star with a higher neutrino flux than our Sun we can follow a simplified assumption of the luminosity constraint and assume star luminosity and total neutrinos emitted (N) is proportional [17].

Furthermore, using futuristic Dyson sphere technologies will allow us to theoretically encompass our sun with a Dyson sphere that consist of neutrino detectors. If we place our Dyson sphere 2.5× the radius of the star away from the center we can get neutrino flux estimates on our detectors [18].

Using one of the most luminous stars in the universe (R136a1 [19]) as a best case example we get:

$$\begin{aligned} \phi_{R136a1} &= \frac{N_{R136a1}}{4\pi(2.5 \times r_{R136a1})^2} \\ \phi_{R136a1} &\approx 2.09 \times 10^{15} m^{-2} s^{-1} \end{aligned} \tag{22}$$

A tried and tested neutrino detector to work from is the Super-Kamiokande detector [20]. We have a 41.4m×39.3m tank full of 5.02×10^7kg of ultra pure water. SK has a detection probability of 8.04×10^{-10} for 10 MeV neutrinos. If our average required gate probability at 10 MeV is 5×10^{-32} then we need $\approx 4 \times 10^{41}$ neutrinos incident on our SK detector.

Since our R136a1's best flux is nowhere near this number we can instead increase the number of SK detectors; requiring 4×10^{22} detectors which will be 1×10^{24}m of SK's back to back and 2×10^{30}kg of ultra pure water required. Furthermore, neutrino's will not be collimated over such a long distance and many will also escape the line of detectors; requiring more SK detectors.

These numbers are incredibly generous yet still very large when put into perspective; showing the resources required for neutrino devices is unfeasible.

VI. CONCLUSIONS

We have calculated neutrino-lepton cross-sections in an attempt to see whether neutrinos would be feasible qubits and in doing so have discovered that their interaction limitations and incredibly small interaction probabilities (thought to be their saving grace) result in an unfeasible number of neutrinos and materials needed to create a probable gate. Probabilistic neutrino-lepton gates are also not possible due to certain neutrino-lepton interactions dominating and therefore failing the universal CNOT requirements.

VII. ACKNOWLEDGMENTS

We'd like to thank Loughborough University's department of Physics and it's students, for providing materials and interesting discussions over the course of this year. Further thanks to Dr. Zagoskin for proposing the idea and supervising the project.

[1] David G. Cory, Amr F. Fahmy, and Timothy F. Havel. Ensemble quantum computing by nmr spectroscopy. *Proceedings of the National Academy of Sciences*, 94(5):1634–1639, 1997.

[2] J. Brooke, D. Bitko, T.F. Rosenbaum, and G. Aeppli. Quantum annealing of a disordered magnet. *Science*, 284(5415):779–781, 1999.

[3] B. Kane. A silicon-based nuclear spin quantum computer. *Nature*, 393:133–137, 1998.

[4] Pieter Kok, W. J. Munro, Kae Nemoto, T. C. Ralph, Jonathan P. Dowling, and G. J. Milburn. Linear optical quantum computing with photonic qubits. *Rev. Mod. Phys.*, 79:135–174, Jan 2007.

[5] David P. DiVincenzo. The physical implementation of quantum computation. *Fortschritte der Physik*, 48(9-11):771–783, 2000.

[6] B. Pontecorvo. Neutrino experiments and the problem of conservation of leptonic charge. *Soviet Physics JetP*, 26(5):984–988, May 1968.

[7] C. L. Cowan, F. Reines, F. B. Harrison, H. W. Kruse, and A. D. McGuire. Detection of the free neutrino: a confirmation. *Science*, 124(3212):103–104, 1956.

[8] Q. R. Ahmad, R. C. Allen, J. M. Wouters, M. Yeh, et al. Measurement of the rate of $\nu_e + d \rightarrow p + p + e^-$ interactions produced by ^8b solar neutrinos at the sudbury neutrino observatory. *Phys. Rev. Lett.*, 87:071301, Jul 2001.

[9] C. A. Argüelles and B. J. P. Jones. Neutrino oscillations in a quantum processor. *Phys. Rev. Research*, 1:033176, Dec 2019.

[10] Tia Miceli Fermilab. Neutrino oscillations, 2014.

[11] P. Adamson, K. Anderson, M. Andrews, R. Andrews, I. Anghel, D. Augustine, A. Aurisano, S. Avvakumov, D.S. Ayres, B. Baller, et al. The numi neutrino beam. *Nuclear Instruments and Methods in Physics Research Section A: Accelerators, Spectrometers, Detectors and Associated Equipment*, 806:279–306, Jan 2016.

[12] Bruce A. Campbell and Ahmed Ismail. Leptonic pion decay and physics beyond the electroweak standard model, 2008.

[13] J. A. Formaggio and G. P. Zeller. From ev to eev: Neutrino cross sections across energy scales. *Rev. Mod. Phys.*, 84:1307–1341, Sep 2012.

[14] G.'t Hooft. Prediction for neutrino-electron cross-sections in weinberg's model of weak interactions. *Physics Letters B*, 37(2):195–196, 1971.

[15] A Oralbaev, M Skorokhvatov, and O Titov. The inverse beta decay: a study of cross section. *Journal of Physics: Conference Series*, 675(1):012003, Feb 2016.

[16] Kevin McFarland. Neutrino interactions, 2008.

[17] Diego Vescovi, Carlo Mascaretti, Francesco Vissani, Luciano Piersanti, and Oscar Straniero. The luminosity constraint in the era of precision solar physics. *Journal of Physics G: Nuclear and Particle Physics*, 48(1):015201, nov 2020.

[18] Jason Wright. Dyson spheres. *Serbian Astronomical Journal*, (200), 2020.

[19] Joachim M Bestenlehner, Paul A Crowther, Saida M Caballero-Nieves, Fabian R N Schneider, Sergio Simón-Díaz, Sarah A Brands, Alex de Koter, Götz Gräfener, Artemio Herrero, Norbert Langer, and et al. The r136 star cluster dissected with hubble space telescope/stis – ii. physical properties of the most massive stars in r136. *Monthly Notices of the Royal Astronomical Society*, 499(2):1918–1936, Sep 2020.

[20] S. Fukuda et al. The super-kamiokande detector. *Nuclear Instruments and Methods in Physics Research Section A: Accelerators, Spectrometers, Detectors and Associated Equipment*, 501(2):418–462, 2003.

VIII. APPENDIX: FIGURES

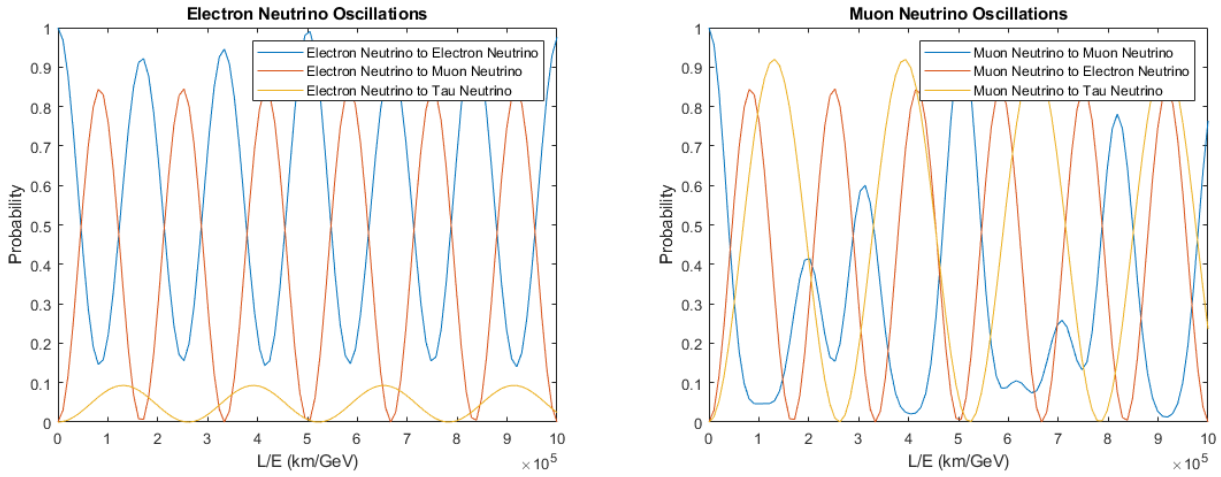

FIG. 5. Oscillation Probabilities as a function of L/E

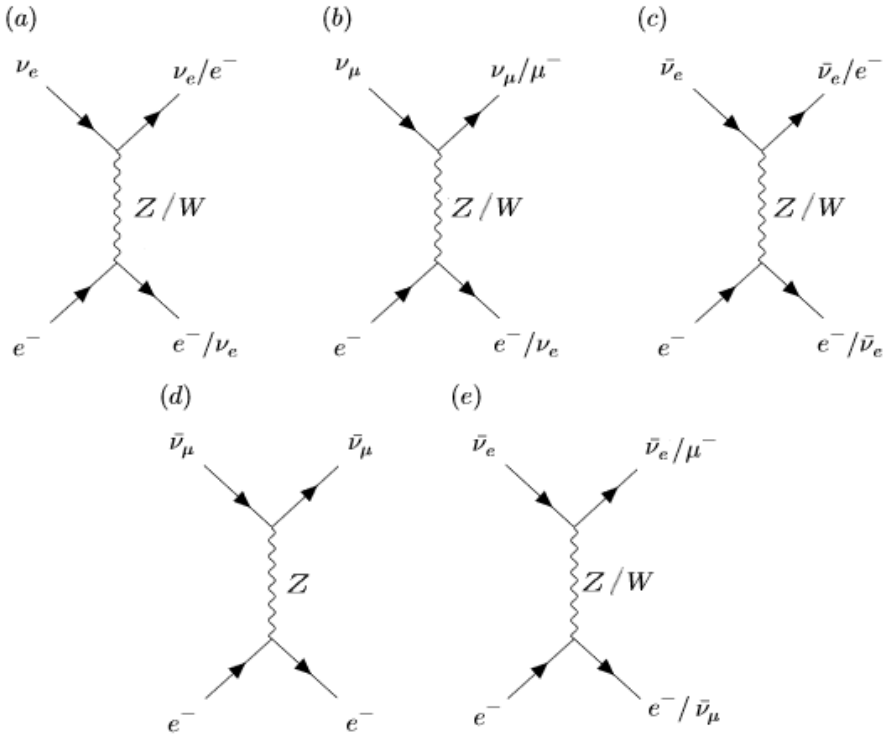

FIG. 6. shows Feynman diagram interactions of neutrinos and antineutrinos with target electrons following both neutral current (Z boson) or charged current (W boson) paths.
(a) $\nu_e + e^- \rightarrow \nu_e \ / \ e^- + e^- \ / \ \nu_e$, (b) $\nu_\mu + e^- \rightarrow \nu_\mu \ / \ \mu^- + e^- \ / \ \nu_e$, (c) $\overline{\nu}_e + e^- \rightarrow \overline{\nu}_e \ / \ e^- + e^- \ / \ \overline{\nu}_e$, (d) $\overline{\nu}_\mu + e^- \rightarrow \overline{\nu}_e + e^-$, (e) $\overline{\nu}_e + e^- \rightarrow \overline{\nu}_e \ / \ \mu^- + e^- \ / \ \overline{\nu}_\mu$.

IX. APPENDIX: TABLES

Input (a)	Input (b)	Output (c)	Output (d)	Probability
e	e	e	e	6.07×10^{-16}
e	e	e	μ	2.24×10^{-15}
e	e	μ	e	2.24×10^{-15}
e	e	μ	μ	8.27×10^{-15}
e	μ	e	μ	1.05×10^{-16}
e	μ	e	e	1.09×10^{-17}
e	μ	μ	μ	3.88×10^{-16}
e	μ	μ	e	4.02×10^{-17}
μ	e	μ	μ	3.88×10^{-16}
μ	e	μ	e	1.05×10^{-16}
μ	e	e	e	1.09×10^{-17}
μ	e	e	μ	4.02×10^{-17}
μ	μ	μ	e	1.89×10^{-18}
μ	μ	μ	μ	1.82×10^{-17}
μ	μ	e	μ	1.89×10^{-18}
μ	μ	e	e	1.96×10^{-19}
$\overline{e}$	$\overline{e}$	$\overline{e}$	$\overline{e}$	6.74×10^{-17}
$\overline{e}$	$\overline{e}$	$\overline{e}$	$\overline{\mu}$	1.21×10^{-18}
$\overline{e}$	$\overline{e}$	$\overline{\mu}$	$\overline{e}$	1.21×10^{-18}
$\overline{e}$	$\overline{e}$	$\overline{\mu}$	$\overline{\mu}$	2.18×10^{-20}
$\overline{e}$	$\overline{\mu}$	$\overline{e}$	$\overline{\mu}$	2.82×10^{-17}
$\overline{e}$	$\overline{\mu}$	$\overline{e}$	$\overline{e}$	2.49×10^{-16}
$\overline{e}$	$\overline{\mu}$	$\overline{\mu}$	$\overline{\mu}$	5.07×10^{-19}
$\overline{e}$	$\overline{\mu}$	$\overline{\mu}$	$\overline{e}$	4.47×10^{-18}
$\overline{\mu}$	$\overline{e}$	$\overline{\mu}$	$\overline{\mu}$	5.07×10^{-19}
$\overline{\mu}$	$\overline{e}$	$\overline{\mu}$	$\overline{e}$	2.82×10^{-17}
$\overline{\mu}$	$\overline{e}$	$\overline{e}$	$\overline{e}$	2.49×10^{-16}
$\overline{\mu}$	$\overline{e}$	$\overline{e}$	$\overline{\mu}$	4.47×10^{-18}
$\overline{\mu}$	$\overline{\mu}$	$\overline{\mu}$	$\overline{e}$	1.04×10^{-16}
$\overline{\mu}$	$\overline{\mu}$	$\overline{\mu}$	$\overline{\mu}$	1.18×10^{-17}
$\overline{\mu}$	$\overline{\mu}$	$\overline{e}$	$\overline{\mu}$	1.04×10^{-16}
$\overline{\mu}$	$\overline{\mu}$	$\overline{e}$	$\overline{e}$	9.19×10^{-16}

TABLE II. Cross-sections of (anti)neutrino with target electrons and muons in a two qubit system for input neutrino energy $E_\nu = 100$ GeV.